International Journal of the Physical Sciences Vol. 6(28), pp. 6422-6438, 9 November, 2011
Available online at http://www.academicjournals.org/IJPS
DOI: 10.5897/IJPS11.475
ISSN 1992 - 1950 ©2011 Academic Journals

Full Length Research Paper

Optimum louver angle design for a louvered fin heat exchanger

Jiin-Yuh Jang* and Ying-Chi Tsai

Department of Mechanical Engineering, National Cheng-Kung University, Tainan 70101, Taiwan.

Accepted 14 September, 2011

This paper suggests a method for finding the optimal louver angle of a fin heat exchanger by use of a simplified conjugate-gradient method (SCGM) and a three-dimensional computational fluid dynamics model. The search for optimum louver angles ranging from $\theta = 15^{o}$ to 45^{o} for suitable louver pitches and fluid input velocity are carried out for Reynolds number Re_H (based on the fin spacing 1.5 mm and the frontal velocity 1 to 5 m/s) ranging from 100 to 500. The area reduction of using louver surface relative to the plain surface is the objective function to be maximized. The model calculates optimum performance of the heat-exchanger by means of finding the fin angle which would give the biggest reduction in area of the louvered surfaces relative to plain fin surfaces required to give equivalent performance. The numerical optimizer adjusts the angle of the louvered fin toward the maximization of the performance of the heat exchanger. Additionally, the correlations of the optimal louver angle as function of Reynolds number Re_H are obtained.

Key words: Heat transfer, louvered fin, optimization, simplified conjugate-gradient method.

INTRODUCTION

Heat exchangers are used in a wide variety of applications. Typical among them are the district heat stations, HVAC (heating, ventilating, air-conditioning, and refrigeration) systems, food and chemical process systems, and heat recovery systems. Fin and tube heat exchangers are frequently used in vehicular air-conditioning systems in the automotive industry. An advantage of decreasing the size of heat exchangers in vehicles is weight savings, as well as a reduction in the required frontal area of the vehicles that must be dedicated to the heat exchanger. Therefore, enhanced surfaces are often employed to effectively improve the overall performance of the fin and tube heat exchanger.

The design of louvered fins as applied in heat exchangers has been extensively studied experimentally with the first reliable data published by Kays and London (1950), and more recently, numerically with computational finite volume methods. Such heat exchangers are characterized by having fins that have been cut and bent out into the flow stream at frequent intervals. The purpose of having louvers is to break up the boundary layers so as to yield higher heat transfer coefficients and lower thermal resistance than that which are possible with plain fins under the same flow conditions. As a general rule, the more frequent the interruption, the higher the heat transfer rate, although the friction factor is also increased.

Investigations into louvered fin heat exchangers are principally divided into three categories. Firstly, for louvered fins having flat tube configurations, extensive experimental data were reported by Davenport (1983), Achaichia (1987) and Achaichia and Cowell (1988). Webb and Jung (1992) presented experimental data for six brazed aluminum heat exchangers. Rugh et al. (1992) experimentally studied a high fin density louver surface. Sunden and Svantesson (1990) found that every configuration of louvered surfaces they studied were more efficient than the corresponding plain surface, and the standard louvered fin geometry revealed higher Stanton number than other inclined louver geometries. Chang and Wang (1996) presented 27 samples of corrugated louvered fin heat exchangers with different geometrical parameters, including louver length, louver pitch, fin height and fin pitch. Webb et al. (1995) developed

*Corresponding author. E-mail: jangjim@mail.ncku.edu.tw. Tel: +886-6-2757575 ext. 62148. Fax: +886-6-2088573.

semi-analytical heat transfer and friction correlations for louvered fin geometry. Chang and Wang (1997) used a data bank consisting of 91 samples to develop a generalized heat transfer correlation for louvered fin geometry.

Secondly, several kinds of experiments where the sizes of the components were scaled up by ten or twenty times have been used both for qualitative flow pattern visualization and local heat transfer measurements. Smoke traces or dye injection techniques as performed by Cowell et al. (1995) revealed the importance of the Reynolds number in characterizing flow patterns which could be described in terms of duct directed or louver directed flows, depending on the Reynolds number. Cowell also used the Reynolds number based on louver pitch (L_p) rather than on the hydraulic diameter, and this reference length (L_p) is now widely used in louvered fin investigations. Cowell found that the flow within the louver array is governed by laminar boundary layer growth and renewal, where at low Reynolds numbers, the layers are so thick that the gap between adjacent louvers is blocked and flow is duct directed, along the line of the fins. At higher Reynolds numbers, the boundary layers are thinner and the flow is almost aligned with the louvers. Antoniou et al. (1990) performed hot-wire measurements of mean velocity and root mean square (r.m.s.) velocity fluctuation in a scaled-up model, and showed that the flow remains laminar and steady for Re_{Lp} (Reynolds number based on louver pitch) up to 1300. For Re_{Lp} > 1300, the velocity fluctuates downstream of the first one or two louvers. DeJong and Jacobi (2003) used the naphthalene sublimation technique and complementary flow visualization to study the effects of boundary walls on flow and heat transfer in louvered-fin arrays and found that at low Reynolds numbers (Re ≈ 600 and below), large separation zones caused a decrease in heat transfer up to 50% compared to that for plain-fin arrays. Nevertheless, if the Reynolds number is high enough to promote unsteady flow near the wall, the net effect is to locally increase heat transfer by approximately 15% (at Re = 1400).

Thirdly, theoretical studies of the physical phenomena in the louvered fin provide detailed information which might not be easily obtained by experiment. Since the early 1980's, numerous attempts have been made to develop two-dimensional models of louvered fin surfaces. Initially, the models were based on the assumption of zero fin thickness and steady laminar two-dimensional flow with periodic boundary conditions. Kajino and Hiramatsu (1987) solved the stream function and vorticity equations for two dimensional, incompressible, steady and laminar flow over flat louvered fins using finite difference methods. A more comprehensive study was carried out by Achaichia and Cowell (1988). They modeled only one louver in a fully developed flow region by assuming cyclic boundary conditions.

In the 1990's, several researchers developed CFD code based on non-orthogonal, boundary-fitted meshes to compute the flow over louvered fins. Suga et al. (1990) and Suga and Aoki (1991) used a rectangular flow domain filled with overlapping Cartesian meshes to compute the flow and heat transfer over a finite-thickness fin. Hiramatsu et al. (1990) and Ikuta et al. (1990) used a block-structured mesh with individual blocks for each louver. Through using the results of their theoretical study, the mechanisms of mass and heat transport reaction phenomena taking place in physical applications can be clarified, and the cost and design time in the product development period may be significantly reduced.

Numerical investigations into the 2D and 3D flow and heat transfer through louvered finned-tube heat exchangers were been performed by Atkinson et al. (1998) and Liu et al. (2000). Jang et al. (2001) investigated three-dimensional convex louvered finned-tube heat exchangers. The effects of different geometrical parameters, including convex louver angles (θ = 15.5, 20.0 and 24.0°), louver pitch (L_p = 0.953 and 1.588 mm) and fin pitch (8, 10 and 15 fins/in.) were investigated in detail.

Although other studies on louvered fins have been made, they are mostly based on the assumption that the louver angle is uniform and constant. Hsieh and Jang (2006) proposed successively increasing or decreasing the louver angle of adjacent louvers and carried out a 3-D numerical analysis on heat and fluid flow. Their results indicated that varying the louver angles applied in heat exchangers could effectively enhance their heat transfer performance. They also showed that the maximum area reduction in their "case B" (+4°) could reach up to 25.5% compared to a plain fin surface.

Recently, AlEssa et al. (2009) performed a study to analyze the enhancement of natural convection heat transfer from a horizontal rectangular fin embedded with rectangular perforations of aspect ratio of two has been examined using finite element technique. Also, the heat transfer enhancement of the perforated fin increases as the fin thickness and thermal conductivity increase. Goodarzian et al. (2011) presented an analytical solution to the problem of the efficiency of straight fins of different configurations when subjected to simultaneous heat and mass transfer mechanisms.

Experimental studies aimed at optimizing louvered fin geometries tend to be costly and time-consuming because of the large number of geometrical parameters involved (for example, louver angle, louver pitch, louver length and fin spacing). Accordingly, the present study uses a numerical optimization technique in the geometrical optimization of louvered fins in order to obtain optimal performance balancing efficient heat transfer with reasonable pressure drops. To reach this goal, the simplified conjugate-gradient method (SCGM, 2010) was combined with a commercial CFD code ANSYS FLUENT (2009) to build an optimizer for finding the best angles of

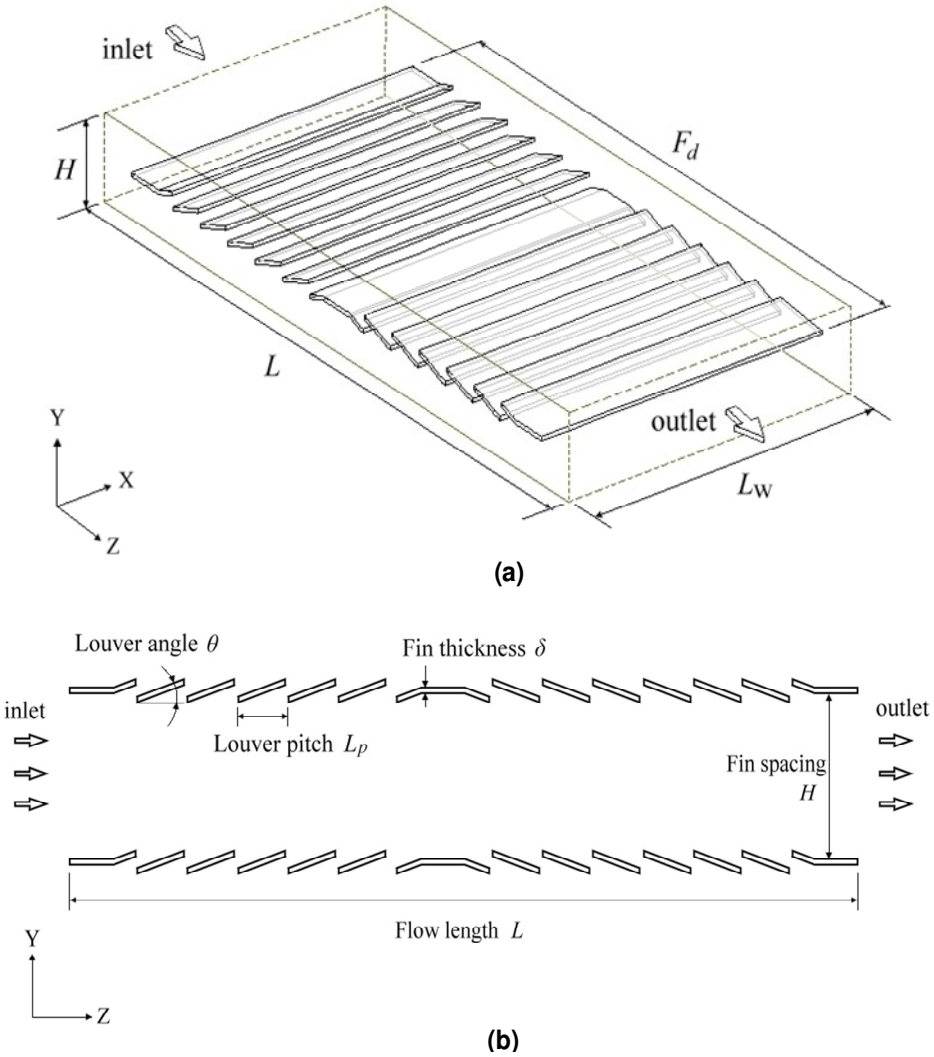

Figure 1. Schematic of the computational domain; (a) definition of geometrical parameters for a multi-louvered fin heat exchanger, (b) cross-section of louvered fin geometry.

the louvered fins. Using the optimizer, the louver angle is adjusted to maximize the performance of the heat exchanger.

MATHEMATICAL ANALYSIS

Figure 1a shows the physical model and computation domain for the louvered fin heat exchanger in Cartesian coordinates. The 3D computational domain is composed of a louvered fin cross-section with entry region, five louvers on either side of the turnaround louver and outlet region as seen from Figure 1b.

Governing equation

In the present study, simulations are performed for Reynolds numbers Re_H (based on the fin spacing 1.5 mm and the frontal velocity, V_{fr}, 1 - 5 m/s) ranging from 100 to 500. This is equivalent to Reynolds number range based on louver pitch (Re_{Lp}) of 66 to 333. As outlined in the previously, experimental observations of Antoniou et al. (1990) have shown that the flow is laminar for up to a Reynolds numbers of approximately 1300. Therefore, the fluid is considered incompressible with constant properties and the flow is assumed to be laminar, steady, three-dimensional and with no viscous dissipation. The dimensionless equations for mass, momentum (Reynolds-averaged Navier-Stokes equation) and energy may be expressed in tensor form as:

$$\frac{\partial U_i}{\partial X_i} = 0 \tag{1}$$

$$\frac{\partial}{\partial X_j}\left(U_i U_j\right) = -\frac{\partial P}{\partial X_i} + \frac{1}{Re_H}\left[\nabla^2 U_i\right] \tag{2}$$

$$\frac{\partial}{\partial X_j}\left(\Theta U_j\right) = \frac{1}{Re_H Pr}\left[\nabla^2 \Theta\right] \tag{3}$$

Table 1. Geometrical parameters and operating conditions of the louvered fin.

Fin spacing (H)	1.5 mm
Fin depth (F_d)	15.0 mm
Fin thickness (δ)	0.1 mm
Louver pitch (L_p)	0.7 mm / 1.0 mm / 1.3 mm
Louver width (L_w)	7.3 mm
Louver angle (θ)	15° - 45°

In the Equations 1 to 3, the velocity has been nondimensionlized with the uniform inlet velocity V_{fr} at the channel inlet, all length coordinates with the fin spacing H, and the pressure with ρV_{fr}^2. The dimensionless temperature is defined as $\Theta = (T-T_{in}) / (T_w-T_{in})$. The Reynolds number is $Re_H = V_{fr} \cdot H/v$ and Pr is the Prandtl number, which is set equal to 0.71 (for air) in the present study.

The local heat transfer coefficient h is defined as:

$$h = \frac{q''}{T_w - T_b} \tag{4}$$

where q'' is the local heat flux and T_b is the local bulk mean temperature of the fluid. The local heat transfer coefficient can be expressed in the dimensionless form by the Nusselt number Nu, defined as:

$$Nu = \frac{h \cdot H}{k} = \frac{\partial \left[\frac{\Theta}{\Theta_b} \right]_{wall}}{\partial n} \tag{5}$$

where H is the fin spacing and k is thermal conductivity respectively. $\Theta_b = (T_b-T_{in}) / (T_w-T_{in})$ is the local dimensionless bulk mean temperature, and n is the dimensionless unit vector normal to the wall. The average Nusselt number $\overline{Nu}$ can be obtained by

$$\overline{Nu} = \frac{\int Nu \quad dA}{\int dA} \tag{6}$$

where dA is the infinitesimal area of the wall surface.

The heat transfer coefficient and the pressure drop can be expressed as the Colburn factor j and the friction factor f which are defined as:

$$j = \frac{\overline{Nu}}{Re_H Pr^{1/3}} \tag{7}$$

$$f = \frac{p_{in} - p}{\frac{1}{2}\rho V_{fr}^2} \times \frac{H}{4L} \tag{8}$$

where pin is the pressure at inlet and L is the flow length. The detailed geometrical for the calculation are given in Table 1.

Boundary conditions

Because the governing equations are elliptic in spatial coordinates, the boundary conditions are required for all boundaries of the computation domain. For the pattern of computation domain shown in Figure 2, no-slip conditions and constant wall temperature T_w are specified at the louvered fin surface. However, one more pair of boundary conditions for the velocity and thermal fields needs to be specified on the periodic interface of fluid between the successive fins. At the upstream boundary, uniform flow with the velocity V_{fr} (1-5 m/s) and temperature T_{in}. On the other hand, at the downstream end of the computational domain, streamwise gradient (Neumann boundary conditions) for all the variables are set to zero. On the symmetry planes (two Y-Z planes), normal gradients are set to zero. On the upper and lower X-Z planes, periodic boundary conditions are imposed.

At the symmetric boundary: (X=*0* and X=L_w)

$$U = \frac{\partial V}{\partial X} = \frac{\partial W}{\partial X} = \frac{\partial \Theta}{\partial X} = 0$$

At the periodic boundary: (Y=*0* and Y=*H*)

$$U, V, W, \Theta(X, 0, Z) = U, V, W, \Theta(X, H, Z)$$

Performance evaluation criteria (PEC)

Many performance evaluation criteria (PEC) have been developed for evaluating the performance of heat exchangers. The VG-1 (variable geometry) performance criteria, as described by Webb (1994), represents the possibility of surface area reduction by using enhanced surfaces having fixed heat duty, temperature difference and pumping power.

$$\frac{h A}{h_{ref} A_{ref}} = \frac{j}{j_{ref}} \frac{A}{A_{ref}} \frac{G}{G_{ref}} \tag{9}$$

where the subscripts of '*ref*' refer to reference plate fin and G is the mass velocity. The pumping power is calculated as

$$\omega = \left(f \frac{A}{A_m} \frac{G^2}{2\rho} \right) \left(\frac{G A_m}{\rho} \right) \tag{10}$$

where A_m is the flow area at minimum cross section. The pumping power ratio relative to the reference plane fin can be obtained by

$$\frac{\omega}{\omega_{ref}} = \frac{f}{f_{ref}} \frac{A}{A_{ref}} \left(\frac{G}{G_{ref}} \right)^3 \tag{11}$$

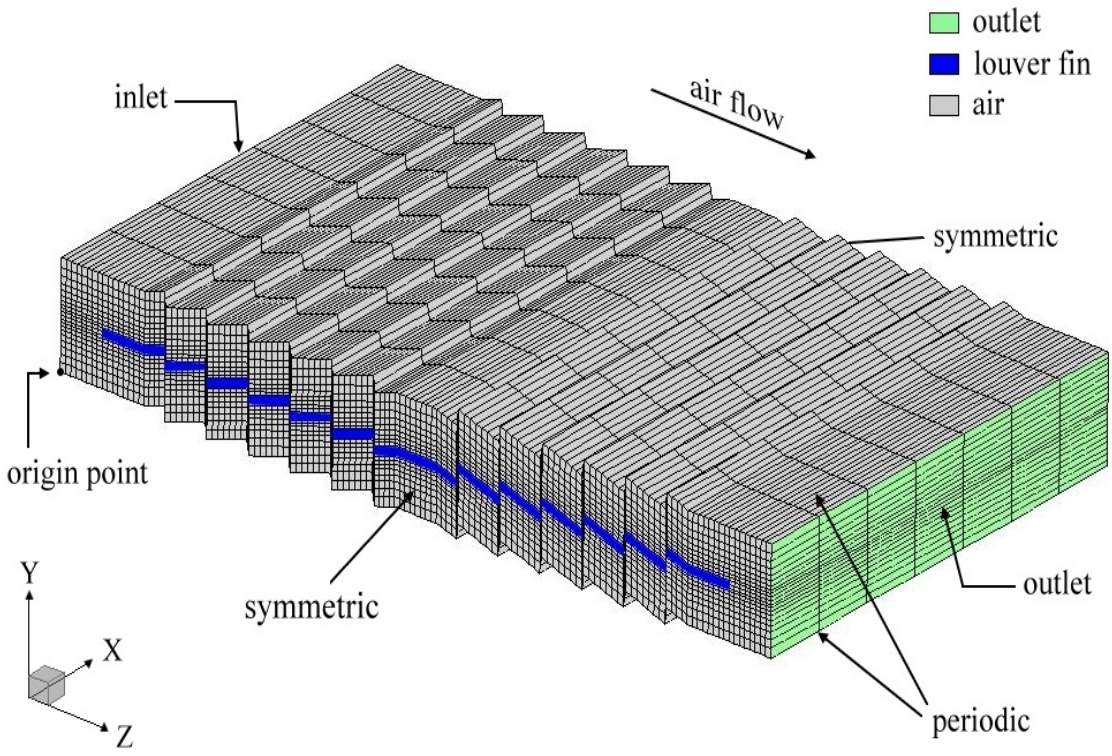

Figure 2. Computational grid system and boundary conditions.

$$\frac{\omega}{\omega_{ref}} = \frac{f}{f_{ref}} \frac{A}{A_{ref}} \left(\frac{G}{G_{ref}} \right)^3 \tag{11}$$

Elimination of the term

$$\frac{hA/h_{ref}A_{ref}}{(\omega/\omega_{ref})^{1/3}(A/A_{ref})^{2/3}} = \frac{j/j_{ref}}{(f/f_{ref})^{1/3}} \tag{12}$$

Under the pumping power constraint of case VG-1, that is ($\omega / \omega_{ref} = 1$), we may obtain the area reduction ratio relative to the reference plane fin as

$$\frac{A}{A_{ref}} = \left(\frac{f}{f_{ref}} \right)^{1/2} \left(\frac{j_{ref}}{j} \right)^{3/2} \tag{13}$$

Optimization method

In the present study, the simplified conjugate-gradient method (SCGM) has been combined with ANSYS FLUENT CFD code (2009) as an optimizer for designing the louver angle with louvered fin. Using the optimizer, the uniform angle of the louvered fin is adjusted toward the maximization of the area reduction ratio compared with the fin and tube heat exchanger.

In the simplified conjugate-gradient method, the objective function *J*) in conjunction with the optimization process for the angle of the louvered fin is defined in the following:

Find $$X = \{X_1, X_2, \ldots X_N\}^T \tag{14a}$$

To maximize $$J(X_i) = 1 - A/A_{ref} \tag{14b}$$

Subject to $$X_i^L \le X_i \le X_i^U \quad \text{for } i=1, N \tag{14c}$$

where X represents the design variable vector and N is the number of design variables. $J(X_i)$ is the objective function, which depends on the values of the design variables. X_i^L and X_i^U denote the lower and upper bounds of the design variables respectively, and they simply limit the region of search for the optimization. This leads to an optimal design having a higher performance.

In the present work, louver angle (θ) is selected as the design variable. The optimum design of the heat exchanger can be obtained simultaneously when the friction factor (*f*) and the Colburn factor (*j*). Thus, in this work, the pressure drop and the heat transfer rate are adopted as the objective functions which are represented as $J(X_i)$, respectively.

NUMERICAL METHODS

In order to explore the optimal design parameters of a fin-tube heat exchanger with louvered fins, the following three procedures were used: (1) Defining of the parameter in the main program, (for example, louver angle); (2) Evaluation of the objective functions (that is, the flow and thermal fields) by the analyzer; and (3) optimization

by a nonlinear optimization method. These processes were repeated until the optimization was complete and were performed automatically.]

Flow and thermal fields

In this study, the governing equations were solved numerically using a control volume based finite difference method. The numerical methodology is briefly described here. Finite difference approximations were employed to discretize the transport equations onto a non-staggered grid mesh system. A second-order upwind TVD (total variation diminishing) scheme was used to model the convective terms of the governing equations. Second-order central difference schemes were used to calculate the viscous and source terms. The coupling between velocity and pressure was performed with the SIMPLEC algorithm.

A pressure based predictor/multi-corrector solution procedure was employed to enhance the calculations of velocity–pressure coupling and the continuity–satisfied of the flow field. A grid system of 239×46×11 ($N_x \times N_y \times N_z$) grid points was adopted typically in the computation domain as shown in Figure 2. Here, the grid pattern is coarsely displayed for the convenience of the reader to visualize the flow regions. Three grid systems, of 200×40×11, 239×46×11 and 280×80×11 points were tested. It was found that for V_{fr}=2.0 m/s, the relative errors in the local pressure and temperature between the solutions of 239×46×11 and 280×80×11 were less than 3%. Note that prior to the simulations, a careful check for the grid-independence of the numerical solutions was made to ensure the accuracy and validity of the results. Computations were performed on an INTEL Core2 Q9300 2.54G personal computer and typical CPU times were about 5,000 s for each case.

When the results satisfied the following conditions, the solutions were treated as converged ones:

$$R = \sum_{domain} \left| a_{nb}\phi_{nb} + b - a_p\phi_p \right| < 10^{-5} \tag{15a}$$

$$\left| \frac{\phi_{i+1} - \phi_i}{\phi_i} \right| < 10^{-5} \tag{15b}$$

where R represents the residual sum and ϕ is a general dependent. The subscripts i and nb are the number of iterations and the neighborhood grid points, respectively.

Optimization

When the objective function $J(X_i)$ is obtained as the result of calculation of flow and thermal fields by the analyzer, the main program calls the optimizer to proceed with optimization. Different combinations of these variables represent different designs, among which the optimal one is to be found. At first, the SCGM method evaluates the gradient functions of the objective function, and then it sets up a new conjugate direction for the updated design variables with the help of a direct numerical sensitivity analysis. The initial guess for the value of each search variable is made, and in the successive steps, the conjugate-gradient coefficients and the search directions are evaluated to estimate the new search variables. The solutions obtained from the direct problem solver are method is described as follows:

Consecutive searching directions: The procedure for applying this then used to calculate the value of the objective function, which is further transmitted back to the optimizer for calculating the

1. Generate an initial guess for the design variables (X_i);
2. Adopt the direct problem solver to predict the velocity, pressure, and temperature fields associated with the latest louver angle, and then calculate the objective function J by Equation 14b.
3. When the value of J reaches a maximum, the optimization process is terminated. Otherwise, proceed to step 4.
4. Determine the gradient functions $(\partial J / \partial X_i)^{(k)}$ by applying a small perturbation (ΔX_i) to each value of (X_i), and calculate the corresponding change in objective function (ΔJ). Then, the gradient function with respect to each value of the design variables (X_i) can be calculated by the direct numerical differentiation as

$$\frac{\partial J}{\partial X_i} = \frac{\Delta J}{\Delta X_i} \tag{16}$$

5. Calculate the conjugate-gradient coefficients $\gamma_i^{(k)}$ and the search directions $\xi_i^{(k+1)}$ for each search variable. For the first step with k=1, $\gamma_i^{(1)} = 0$.

$$\gamma_i^k = \left[\frac{(\partial J / \partial X_i)^k}{(\partial J / \partial X_i)^{k-1}} \right]^2 \tag{17}$$

$$\xi_i^{k+1} = \frac{\partial J^k}{\partial X_i} + \gamma_i^k \xi \tag{18}$$

6. Assign values to the coefficients of descent direction (β_i) for all values of the design variables (X_i). Specifically, those values are chosen by a trial-and-error process. In general, the coefficients of descent direction (β_i) are within the range 0.01 to 0.001.
7. Update the design variables with

$$X_i^{(k+1)} = X_i^{(k)} - \beta_i \xi_i^{(k)} \tag{19}$$

Figure 3 shows the flowcharts of the SCGM optimization process. This process is repeated to reach the maximum of the objective function (J). Nevertheless, this procedure led to a high computational time needed to complete the study.

RESULTS AND DISCUSSION

With the help of the experimental data found in the literature, the ranges of the physical and thermal parameters adopted in our model were decided. The numerical predictions should be compared to and correlate with the experimental data. For this purpose, herein one comparison between the present numerical Figure 4. The calculations were made with the geometry of louver pitch L_p = 1 mm and louver angle θ = 22.0°. The figure presents the results of the heat transfer coefficient and pressure drop, expressed in terms of the Colburn factor (j) and the friction factor (f) as a function of Reynolds number based on louver pitch. It can be seen that the j factor and f factor of the numerical data are in good agreement with those of Davenport (1983) and Kim and

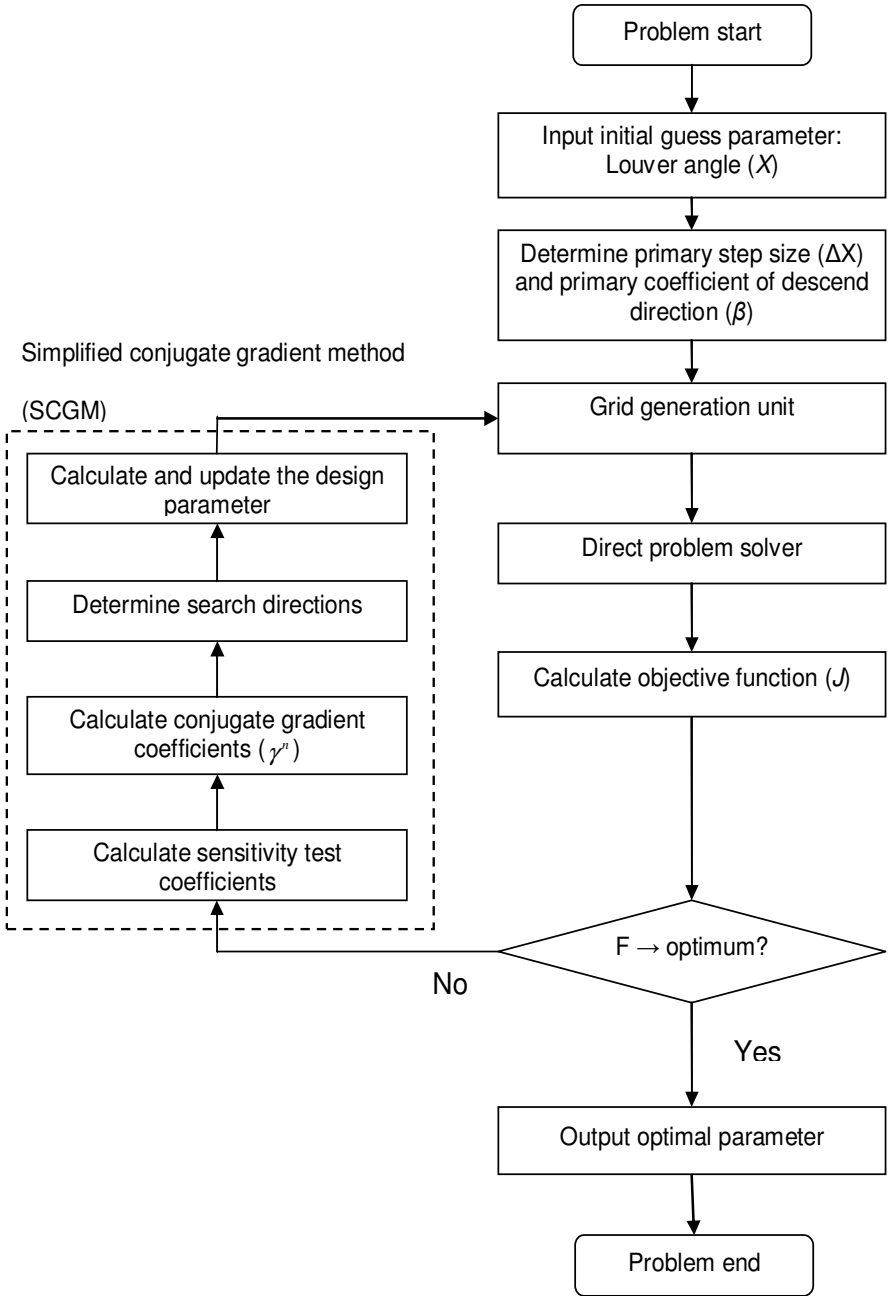

Figure 3. Flowcharts for the optimization method.

and Bullard (2002) within 8%.

The *j* factor and *f* factor for the louvered fin heat exchanger with different louver angles are presented in Figures 5 and 6. Figure 5 shows the results of working with five different Reynolds numbers (Re_H = 100, 200, 300, 400 and 500) based on a constant fin spacing of 1.5 mm for different louver pitches (L_p = 0.7, 1.0 and 1.3 mm). Furthermore, the dimensionless heat transfer coefficient (*j*) is a function of louver angle. It can be seen that when the louver angle is increased, the *j* factor obtains a maximum value. This is because the fluid flow is aligned with the louver at this maximum point on the condition of high Reynolds number. From Figure 5, it can be seen that with the louver pitch set at 0.7 mm, the *j* factor varies more widely with Reynolds number than for greater louver pitches. In addition, the *j* factor decreases when the Reynolds number is increased regardless of louver angle or pitch. With all the different louver pitches, the values of louver angle for maximum *j* points are various. When the Reynolds number equals 100, the louver angles with maximum *j* points are 44, 33 and 25.5° for louver pitch 0.7, 1 and 1.3 mm, respectively. The values

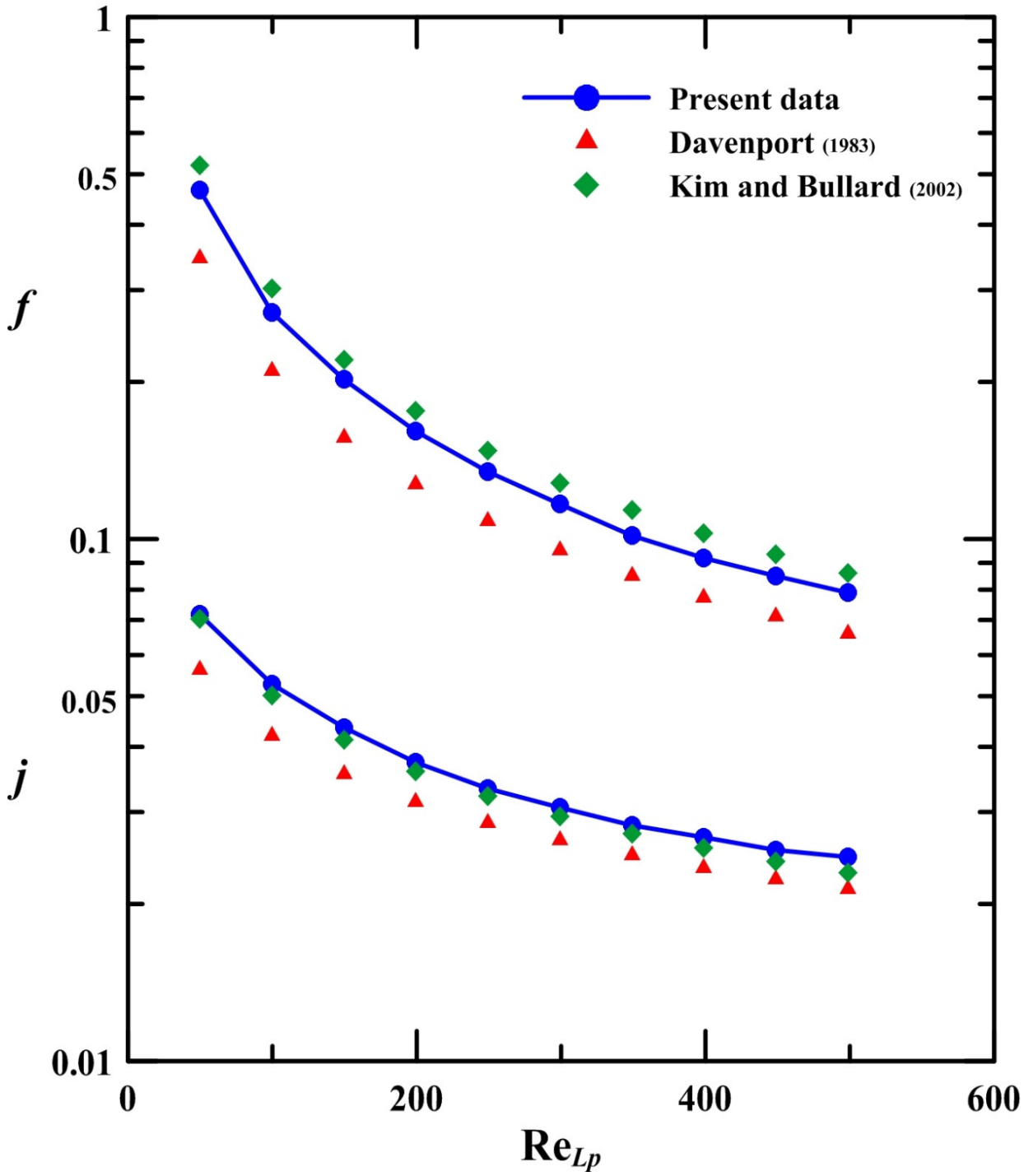

Figure 4. Comparison of present and other correlations for *j*-factor and *f*-factor versus Re_{Lp}.

of optimum louver angle with high heat transfer efficiency are affected by the Reynolds number. Figure 5b illustrates that the optimum louver angles are 33, 27, 24.5, 23.5 and 22° for Reynolds numbers from 100 to 500, respectively. Figure 5a shows that the optimum louver angles are extremely varied (31 to 44°) with different Reynolds numbers when the louver pitch is less than 1 mm. On the contrary, in Figure 5c, the optimum angles have a small range (17 to 26°) when the louver pitch is greater than about 1 mm.

Figure 6 shows the friction factor versus louver angle for different louver pitches (L_p = 0.7, 1.0 and 1.3 mm). The

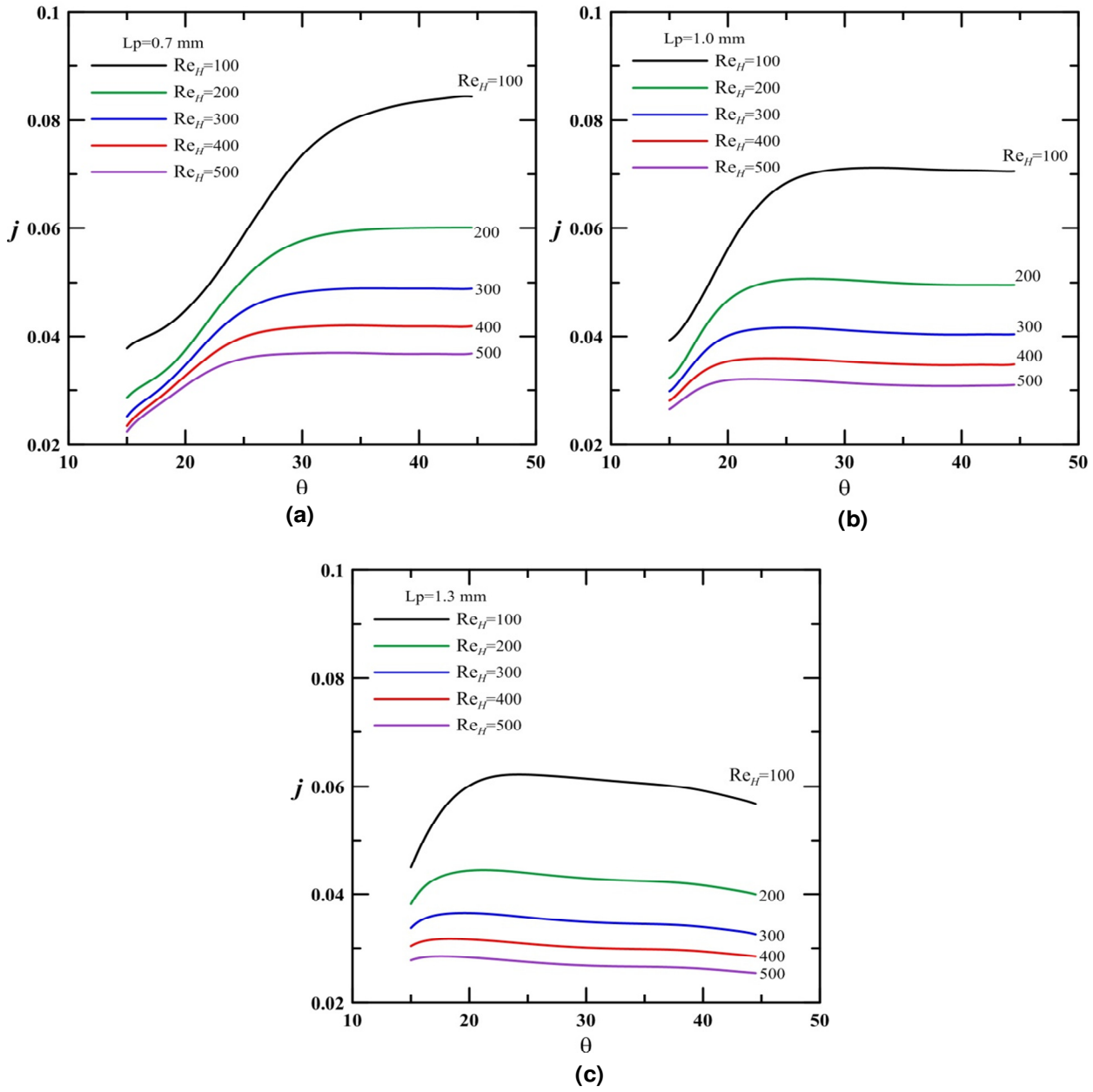

Figure 5. Variation of *j*-factors versus Re_H for different louver angles with; (a) L_p = 0.7 mm (b) L_p = 1mm, and (c) L_p = 1.3 mm.

f factor, which is expressed by pressure drop, always increases with louver angle, but decreases with Reynolds number. The slope of friction factors for all Reynolds numbers becomes smaller with larger louver pitch relatively. In Figure 6a, the effect of louver angle (θ = 45 to 15°) on the *f* factor is increased in *f* factor of 329% for L_p = 0.7 mm under Re_H = 100; similarly, in Figure 6c, the *f* factor is increased but by only 184% under the same conditions for L_p = 1.3 mm. Thus, pressure drops are affected significantly by Reynolds numbers and louver angles. As the louver angle is increased, there is a greater pressure-drop penalty due to drag associated with duct-directed flow, and the path of least resistance becomes louver-directed.

These results reveal that the optimal louver angles with specific louver pitches can be applied in heat exchangers, which would effectively enhance their heat transfer performance. According to previous studies and detailed discussion about pressure drop and heat transfer on various condition of Reynolds number, louver angles and louver pitches, there must exist an optimum value of louver angle. In order to offer a reference design for louvered fin heat exchangers, optimum louver angle searching and correlation equations are also included in

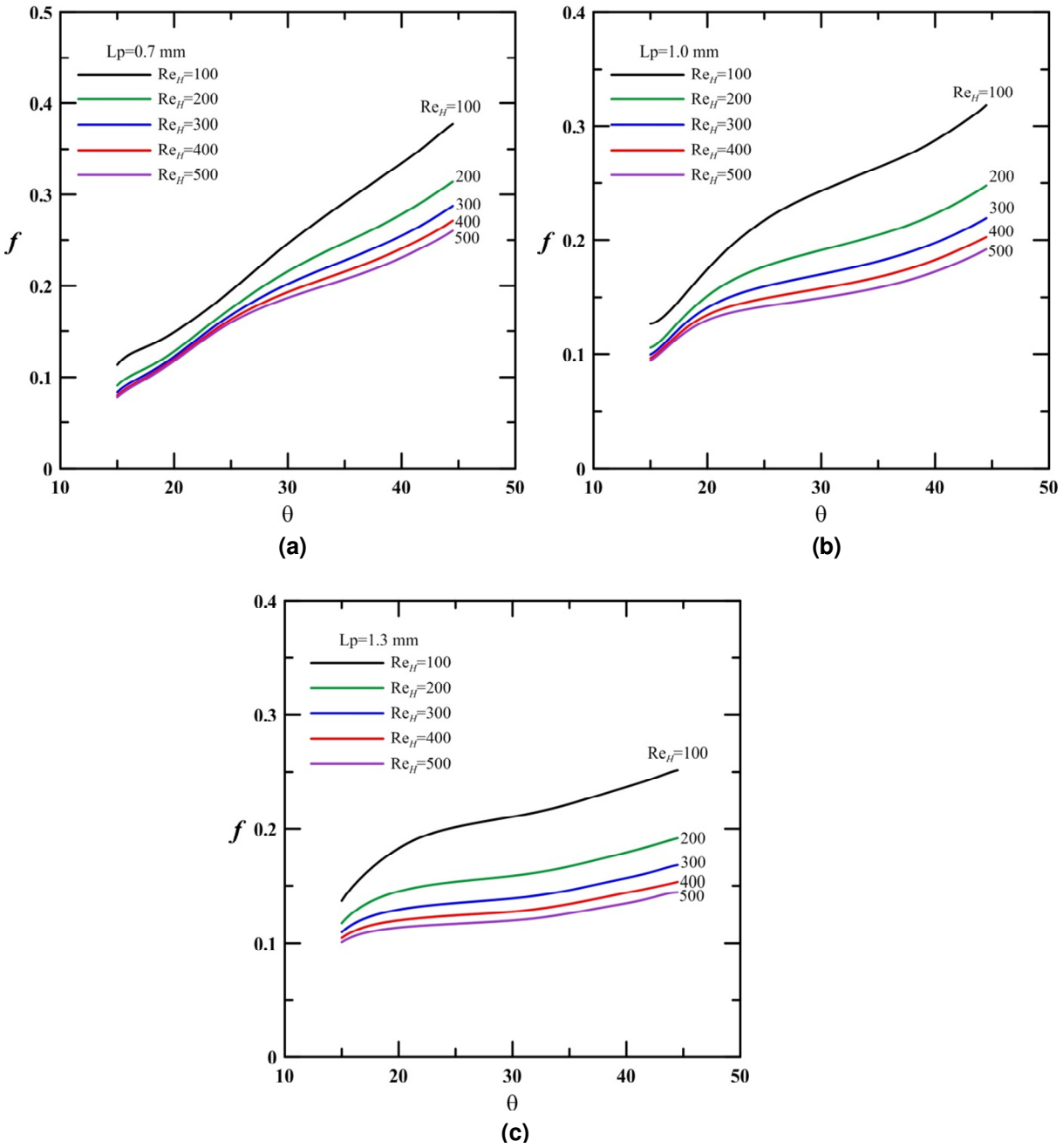

Figure 6. Variation of *f*-factors versus louver angles (θ) for different Re_H with (a) L_p= 0.7 mm (b) L_p = 1 mm, and (c) L_p = 1.3 mm.

this study. For the optimization of the objective function (*J*), the maximum of the area reduction ratio 1-(A/A_{ref}) is chosen as the evaluation criteria, where the subscript '*ref* indicates reference plate fin. The objective function is calculated by the Colburn factor (*j*) and the friction factor (*f*), as shown in Equation 13. One example of the optimization process for the area reduction ratio (Re_H = 300 and L_p = 1.0 mm) is shown in Figure 7. For this case, the area reduction ratio of the optimal design is a substantial improvement of 65.6%. According to the optimizer, the louver angle is searched from 15.0° (original design) to 21.56° (optimum design). In the optimization search process, the magnitude of the area reduction ratio increases rapidly before the 5th iteration, and the maximum value is obtained at the 40th iteration. Moreover, the maximum objective function is almost obtained after the 10th iteration, and the variation in louver angle is not obvious, with angles in the range of 21.5 to

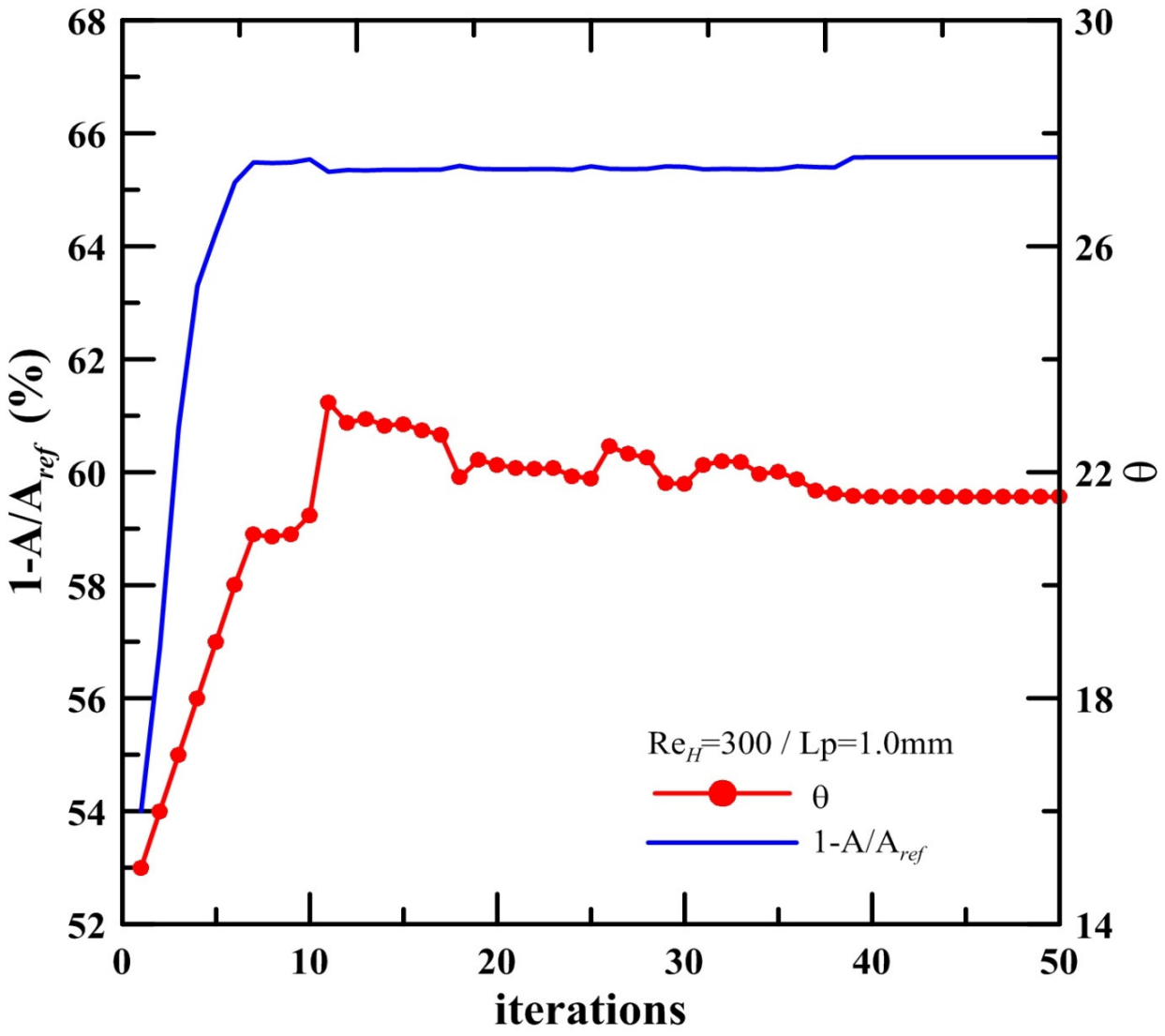

Figure 7. Iteration process for maximum area reduction ratio and louver angle.

22.9° being acceptable. In short, the optimized louvered fin offers better heat transfer performance than the reference plate fin. In addition, as the range of louver angle for the optimum area reduction ratios is between 21.5 to 22.9°, louvers with the optimum louver angle are quite easy to be manufactured due to the tolerance allowed.

In order to understand the effect on heat transfer by variation of louver angle, the solution domain of heat and flow results are discussed in detail as follows. Figure 8 shows multi-colored streamlines which are plotted with velocity magnitude for three different iterations of the optimization process with the flow condition of Re_H = 300 and sections at the central plane (x = 3.7 mm). It appears that the boundary layers expand on both the upper and lower surfaces of the louvers. The relevant heat transfer enhancement is due to thinner boundary layers that form on the leading edge of each louver. Apparently, the upper surface that directly receives the impinging flow may have thinning of the boundary layer, and the lower surface may act as a "diffuser" that thickens the boundary layer. When the louver angle is increased, this effect is more evident.

Figures 9 and 10 present the temperature and pressure distributions, respectively, for three different iterations of the optimization process with Re_H = 300 and x = 3.7 mm (along the symmetric plane). As the louver angle is adjusted toward the maximum heat enhancement, the temperature gradient between the inlet and outlet becomes more pronounced, as shown in Figure 9a to c. Although the optimum value is obtained at 21.5°, the pressure drop is also increased through the optimizer, as seen from Figure 10a and c.

The area reduction ratio for louver angle at three louver

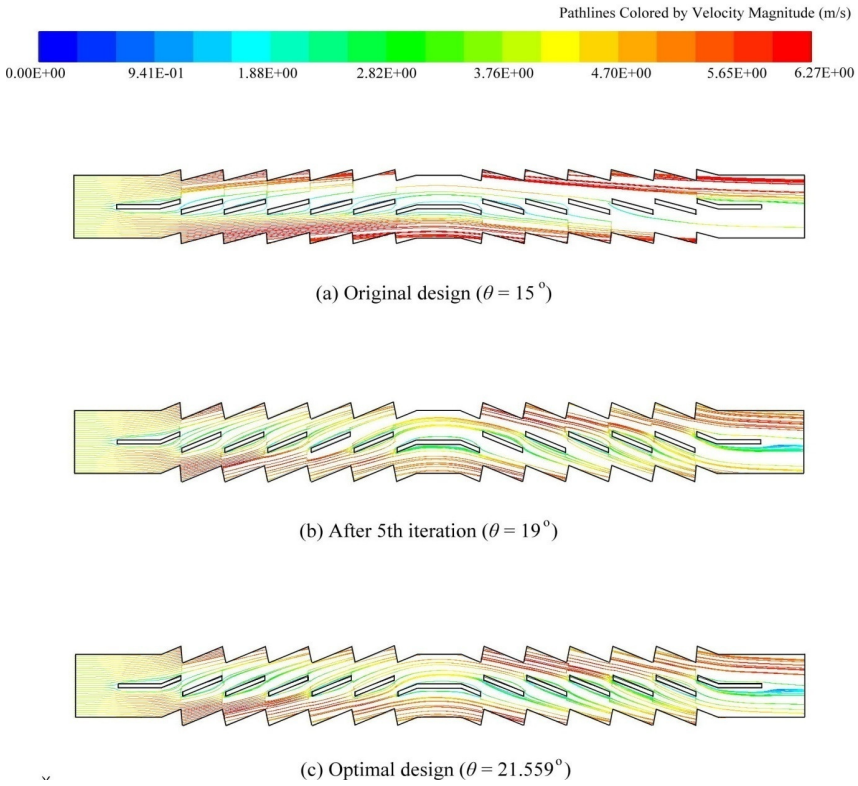

Figure 8. Particle paths distribution for extreme and optimal cases with Re_H = 300 (at the central plane, x = 3.7 mm).

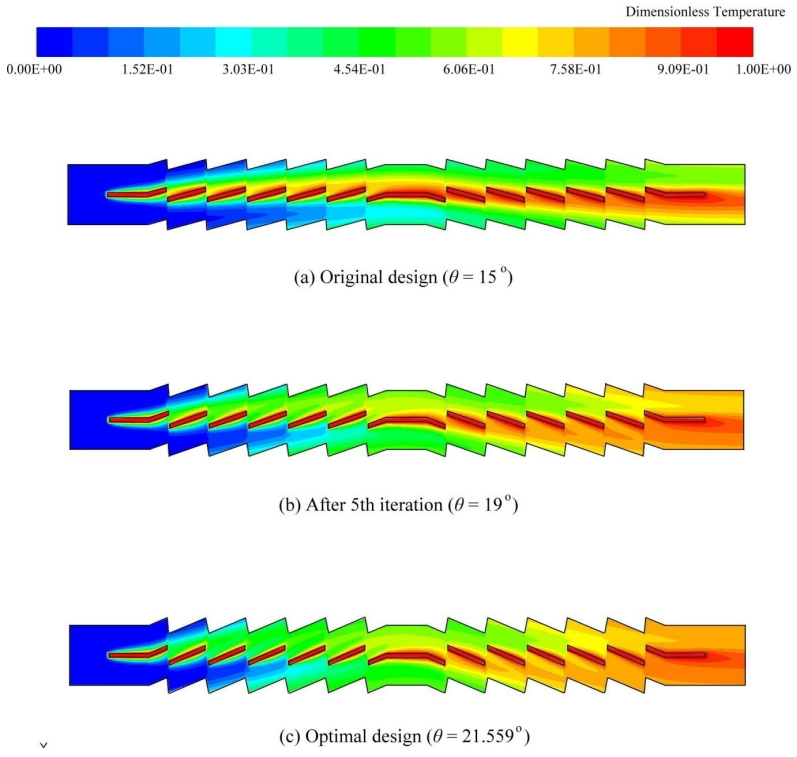

Figure 9. Temperature distribution for extreme and optimal cases with Re_H = 300 (at the central plane, x = 3.7 mm).

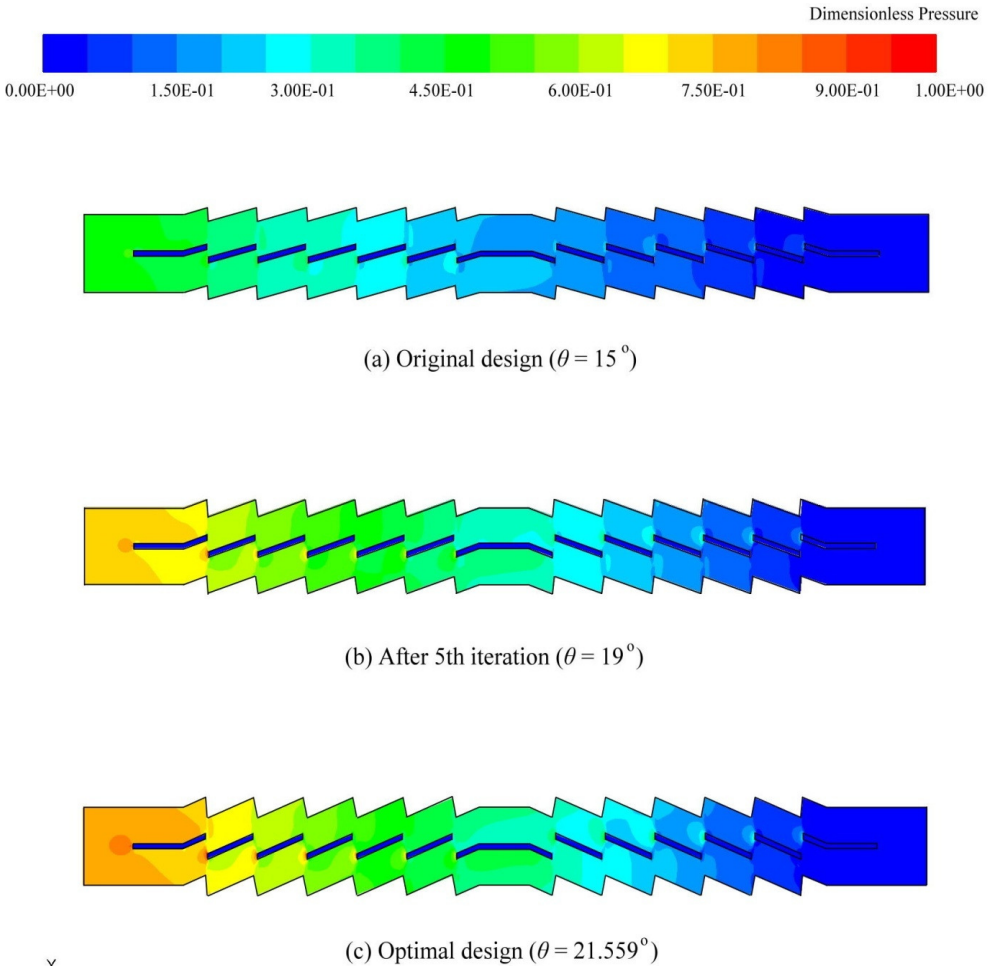

Figure 10. Pressure distribution for extreme and optimal cases with Re_H = 300 (at the central plane, x = 3.7 mm).

pitches (L_p = 0.7, 1 and 1.3 mm) and different Reynolds number is presented in Figure 11. As expected, the area reduction ratio when compared with the reference plate fins are all increased for the cases of Reynolds number ranging from 100 to 500. In Figure 11b, where L_p = 1 mm, there is a maximum for each case with the louver angle ranging from 18 to 28°. It can be seen that the maximum area reduction ratios for Re_H 100 to 500 are 65.3, 66.9, 65.6, 63.7 and 62.2%, respectively; and taking the case Re_H = 100 as an example, the maximum area reduction occurs at louver angle 27.46°. In addition, the optimum value of louver angle with the louver pitch L_p = 0.7 mm is larger than that with L_p = 1 or 1.3 mm, as shown in Figure 11a to c. Additionally, as the Reynolds number is increased, the optimum louver angles are reduced for all three different louver pitches.

From the optimum results found in the study, a correlation for the louver angle can be presented in terms of Reynolds number, as:

$$\theta_{Lp=0.7\,mm} = 96.201\ \mathrm{Re}_H^{-0.218} \quad (20)$$

$$\theta_{Lp=1mm} = 74.433\ \mathrm{Re}_H^{-0.218} \quad (21)$$

$$\theta_{Lp=1.3\,mm} = 61.446\ \mathrm{Re}_H^{-0.218} \quad (22)$$

Through the correlation, the louver angle can be predicted by Reynolds number. Figure 12 illustrates the discrepancy between the values yielded by Equations 20 to 22 and the numerical predictions. In Figure 12, results with the cases listed in Table 2 are presented. It is seen that the maximum relative difference between these two sets of data is within 10%.

Conclusions

In the present work, the optimal geometry of a fin-and-tube heat exchanger with louvered fins for a fixed channel volume is investigated numerically. To calculate the heat transfer rate and pressure drop which are the key parameters, the governing equations are solved by using

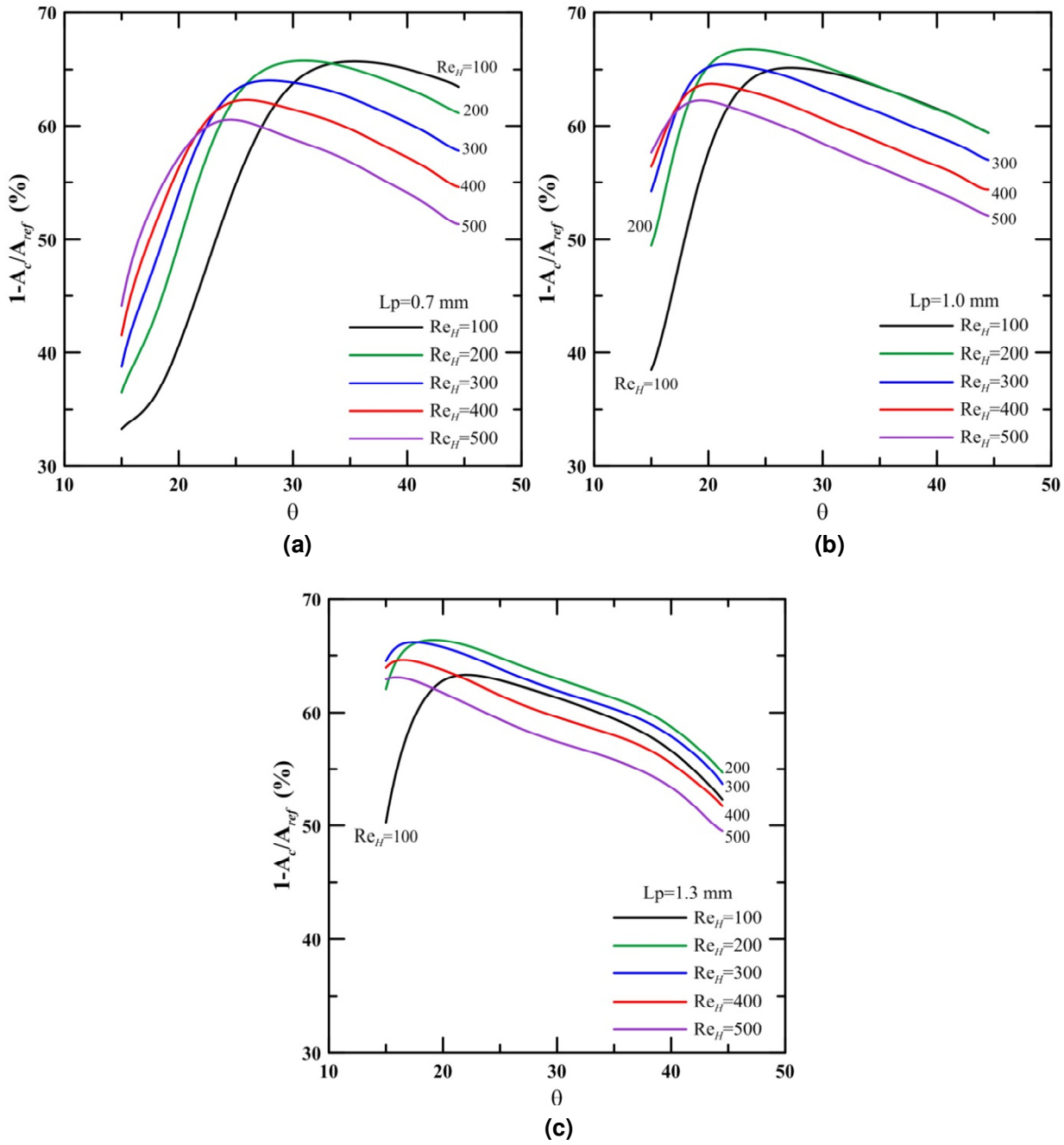

Figure 11. Area reduction ratio versus louver angle (θ) for various Re_H with (a) L_p= 0.7 mm (b) L_p = 1 mm, and (c) L_p=1.3 mm.

the finite volume method. Flow is assumed to be laminar and three-dimensional and a computational domain from the fluid inlet to the outlet is solved directly. In addition, the SCGM method is used to perform the optimization and the objective function problem is evaluated by using the PEC. The major conclusions are summarized as follows:

1. For a louvered fin heat exchanger, both the Colburn factor (j) and friction factor (f) increase firstly with the increase of louver angle for $\theta < 30°$. However, the variation of Colburn factor with greater louver angles is small, but the friction factor always increases for $\theta > 30°$. The objective function can expressed in terms of the Colburn factor (j) and the friction factor (f), and the optimal louver angler can be found by using the PEC.

2. The maximum area reduction ratios of the louvered fins are 65.8, 65.9, 64.0, 62.3 and 60.5% for Re_H 100 to 500 with L_p = 0.7 mm; the results for L_p = 1 mm are 65.3, 66.9, 65.6, 63.7 and 62.2% for Re_H 100 to 500. Finally,

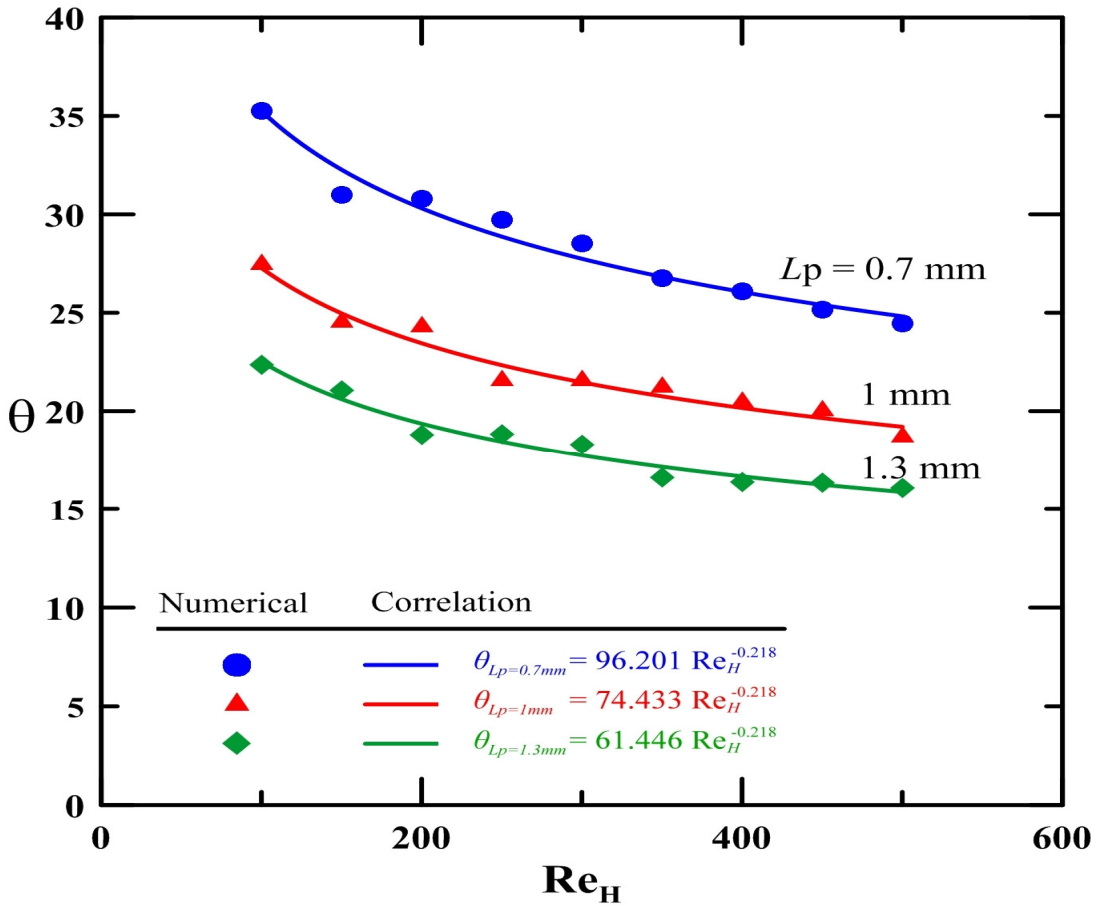

Figure 12. Comparison and correlation of optimal louver angle versus Re_H.

Table 2. Optimized results for different for Re_H =100 to 500 at three louver pitches.

L_p (mm)	Re_H	θ (°)	*Nu*	C_p	*j*	*f*	$1-\frac{A}{A_{ref}}$ (%)
0.7	100	35.264	7.252	8.264	0.0813	0.2951	65.838
	200	30.788	10.418	6.208	0.0584	0.2217	65.892
	300	28.535	12.751	5.411	0.0476	0.1932	64.046
	400	26.086	14.496	4.787	0.0406	0.1710	62.272
	500	24.362	15.869	4.323	0.0356	0.1544	60.477
1.0	100	27.462	6.291	9.285	0.0705	0.2321	65.286
	200	24.229	9.006	6.963	0.0505	0.1741	66.868
	300	21.559	11.018	5.948	0.0411	0.1487	65.579
	400	20.470	12.707	5.454	0.0356	0.1364	63.723
	500	18.687	13.964	4.919	0.0313	0.1230	62.244
1.3	100	22.368	5.528	10.089	0.0620	0.1940	58.384
	200	18.798	7.888	7.357	0.0442	0.1415	66.531
	300	18.219	9.771	6.512	0.0365	0.1252	66.183
	400	16.370	11.248	5.807	0.0315	0.1117	64.658
	500	16.052	12.617	5.502	0.0283	0.1058	63.109

the area reduction ratios with L_p = 1.3 mm are 58.4, 66.5, 66.1, 64.7 and 63.1% for Re_H 100–500, respectively.
3. In the optimization searching process with the conditions of Re_H = 300 and L_p = 1.0 mm, the magnitude of the area reduction ratio increases rapidly before the 5th iteration, and the maximum value is obtained at the 40th iteration. The range of louver angle for the optimum area reduction ratios are between 21.5 and 22.9°, this implies that a heat exchanger with the optimum louver angle can easily be manufactured.
4. When L_p = 0.7 mm, the louver angles for optimum area reduction ratios are 35.26, 30.79, 28.54, 26.09 and 24.36° for Re_H 100 to 500. When L_p = 1 mm, the louver angles for optimum area reduction ratios are 27.46, 24.28, 21.56, 20.47 and 18.69°. Lastly, if L_p = 1.3 mm, the louver angles for optimum area reduction ratios are 22.37, 18.80, 18.28, 16.37 and 16.05°, respectively.
5. The correlation expressions for the optimal louver angle are presented in terms of Reynolds number Re_H (based on the fin spacing). Through the correlations, the optimal louver angle can be calculated and can be applied to the design of heat exchangers.

Nomenclature: A_{fr}, frontal area (m^2); A_m, flow area at minimum cross section (m^2); F, friction factor; F_d, fin depth(mm); G, mass velocity (kg s^{-1} m^{-2}); h, heat transfer coefficient $(W\,m^{-2}K^{-1})$; H, fin spacing (mm); J, Colburn factor; J, objective function; K, thermal conductivity $(W\,m^{-1}K^{-1})$; L, flow length (mm); L_w, louver width (mm); L_p, louver pitch (mm) n, dimensionless unit normal vector; Nu, local Nusselt number, $(h\cdot H)/k$; $\overline{Nu}$, average Nusselt number; p, pressure (Pa); P, dimensionless pressure, $(p_{in}-p)/\rho V_{fr}^2$; Pr, Prandtl number, ν/α; q'', heat flux $(W\ m^{-2})$; R, residual sum; Re_H, Reynolds number, $V_{fr}\cdot H/\upsilon$; T, temperature (K); T_b, bulk mean temperature (K); U_i, U_j, dimensionless velocity vectors; V_{fr}, frontal velocity (m s^{-1}); U, V, W, dimensionless velocity in X, Y and Z directions; X_i, design variable vector; X, Y, Z, Cartesian coordinates.

Greek symbols: α, Thermal diffusivity, (m^2 s^{-1}); β, descend direction coefficient; δ, fin thickness (mm); θ, louver angle; Θ, dimensionless temperature, $(T-T_{in})/(T_w-T_{in})$; Θ_b, dimensionless bulk mean temperature, $(T_b-T_{in})/(T_w-T_{in})$; ρ, density of fluid (kg m^{-3}); ν, kinematic viscosity (m^2 s^{-1}); ξ, search directions; ϕ, general dependent; ω, pumping power.

Subscripts: in, Inlet; ref, reference; W, wall.

ACKNOWLEDGEMENT

Financial support for this work was provided by the National Science Council of Taiwan, under contract NSC99-2221-E-006-141-MY2.

REFERENCES

Achaichia A (1987). The performance of louvered tube-and-plate fin heat transfer surface. PhD dissertation, Brighton Polytechnic, Brighton, UK.

Achaichia A, Cowell TA (1988). Heat transfer and pressure drop characteristics of flat tube and louvered plate fin surfaces. Exp. Thermal Fluid Sci., 1: 147-157.

Al-Essa AH, Maqableh AM, Ammourah S (2009). Enhancement of natural convection heat transfer from a fin by rectangular perforations with aspect ratio of two. Int. J. Phys. Sci., 4(10): 540-547.

ANSYS FLUENT (2009). A Release 12.0, Documentation for ANSYS Workbench. ANSYS Ltd.

Antoniou AA, Heikal MR, Cowell TA (1990). Measurements of local velocity and turbulence levels in arrays of louvered plate fins. Proceed. of the 9th Int. Heat Transfer Conf., Jerusalem, Israel, pp. 105–110.

Atkinson KN, Drakulic R, Heikal MR, Cowell TA (1998). Two-and three-dimensional numerical models of flow and heat transfer over louver fin arrays in compact heat exchangers. Int. J. Heat Mass Transf., 41: 4063–4080.

Chang YJ, Wang CC (1996). Air side performance of brazed aluminum heat exchangers. J. Enhanced Heat Transfer, 3: 15–28.

Chang YJ, Wang CC (1997). A generalized heat transfer correlation for louver fin geometry. Int. J. Heat Mass Transfer, 40: 533–544.

Cowell TA, Heikal MR, Achaichia A (1995). Flow and heat transfer in compact louvered fin surfaces. Exp. Thermal Fluid Sci., 10: 192–199.

Davenport CJ (1983). Correlations for heat transfer and flow friction characteristics of louvered fin. AIChE Symposium series, pp.19–27.

DeJong NC, Jacobi AM (2003). Flow, heat transfer, and pressure drop in the near-wall region of louvered-fin arrays. Exp. Thermal Fluid Sci., 27:237–250.

Goodarzian H, Sahebi SAR, Shobi MO, Safaee J (2011). A collocation solution on the optimization of straight fin with combined heat and mass transfer. Int. J. Phys. Sci., 6(9): 2268-2274.

Hiramatsu M, Ishimaru T, Matsuzaki K (1990). Research on fins for air conditioning heat exchangers. JSME Int. J. Ser. II, 33: 749–756.

Hsieh CT, Jang JY (2006). 3-D thermal-hydraulic analysis for louver fin heat exchangers with variable louver angle. Appl. Thermal Eng., 26: 1629–1639.

Ikuta S, Sasaki Y, Tanaka K, Takagi M, Himeno R (1990). Numerical analysis of heat transfer around louver assemblies. Int. Congress & Exposition Tech., Detroit, Michigan, USA.

Jang JY, Cheng CH, Huang YX (2010). Optimal design of baffles locations with interdigitated flow channels of a centimeter-scale proton exchange membrane fuel cell. Int. J. Heat Mass Transfer, 53: 732–743.

Jang JY, Shieh KP, Ay H (2001). 3-D thermal-hydraulic analysis in convex louver finned -tube heat exchangers. ASHRAE Annual Meeting, Cincinnati, Ohio, USA. pp. 501–509.

Kajino M, Hiramatsu M (1987). Research and development of automotive heat exchangers. Heat Transfer in High Tech. and Power Eng., Hemisphere, Washington DC., USA, pp. 420–432.

Kays WM, London AL (1950). Heat transfer and flow friction characteristics of some compact heat exchanger surfaces-Part I: Test system and procedure. Trans. ASME, 72: 1075–1085.

Kim MH, Bullard CW (2002). Air-side thermal hydraulic performance of multi-louvered fin aluminum heat exchangers. Int. J. Refrigeration, 25: 390–400.

Liu MS, Leu JS, Liaw JS, Wang CC (2000). 3-D simulation of the thermal-hydraulic characteristics of louvered fin-and-tube heat exchangers with oval tubes. ASHRAE Annual Meeting, Minneapolis, Minnesota, USA. pp. 849–855.

Pantaker SV (1981). A Calculation procedure for two-dimensional elliptic

problem. Numerical Heat Transfer, 4: 409-426.
Rugh JP, Pearson JT, Ramadhyani S (1992). A study of a very compact heat exchanger used for passenger compartment heating in automobiles. In Proceeding of Compact Heat Exchangers for Power and Process Industries, ASME Symp. Ser, HTD, 201:15–24.
Suga K, Aoki H (1991). Numerical study on heat transfer and pressure drop in multilouvered fins. In Proceed. of ASME/JSME Thermal Eng. Joint Conf., 4: 361–368.
Suga K, Aoki H, Shinagawa T (1990). Numerical analysis on two dimensional flow and heat transfer of louvered fins using overlaid grids. JSME Int. J. Ser. II, 33: 122–127.
Sunden B, Svantesson J (1990). Thermal hydraulic performance of new multilouvered fins. In Proceeding of the 9th International Heat Transfer Conference pp. 91–96.
Webb RL (1994). Principles of Enhanced Heat Transfer. John Wiley and Sons, New York.
Webb RL, Chang YJ, Wang CC (1995). Heat transfer and friction correlation for the louver fin geometry. Int. J. Heat Mass Transf., 2: 533–541.
Webb RL, Jung SH (1992). Air side performance of enhanced brazed aluminum heat exchangers, ASHRAE Trans., 98: 391–401.